Supplement of Clim. Past, 22, 1711–1727, 2026
https://doi.org/10.5194/cp-22-1711-2026-supplement

Climate of the Past
Open Access

Supplement of

Muted orbital-scale monsoon variability over the Korean Peninsula

Nitesh Sinha et al.

Correspondence to: Nitesh Sinha (nitesh@pusan.ac.kr)

This file includes:

Figures S1 to S16
Section S1-S2
Tables S1 to S3
SI References

Section S1: Tagging Experiment

The water tagging experiment has been conducted with the iCESM, and we used the following source regions (Figure S7):

Land Tagging:

SAS - South Asia, **CAS** - Central Asia, **TAS** - Tropical Asia, **EAS** - East Asia, **NAS** - North Asia, **AFR** - Africa, **EUR** - Europe, **LND** - All land.

Ocean Tagging:

NNP - northern North Pacific, **SNP** - subtropical North Pacific, **EEP** - east equatorial Pacific, **WEP** - west equatorial Pacific, **SSP** - subtropical South Pacific, **EQI** - equatorial Indian, **SSI** - subtropical South Indian.

P is the total precipitation at the target location (KP) with contributions P_i from all the tagged source regions.

$$P = \sum_{i=1}^{n} \mathrm{P_i}$$

$\delta^{18}O_p$ at a particular grid cell is the sum of precipitation-$\delta^{18}O_i$ originating from all tagged source regions (i), weighted by their precipitation contribution:

$$\delta^{18}\mathrm{O_p} = \sum_{i=1}^{n} \delta^{18}\mathrm{O_i}\frac{\mathrm{P_i}}{\mathrm{P}}$$

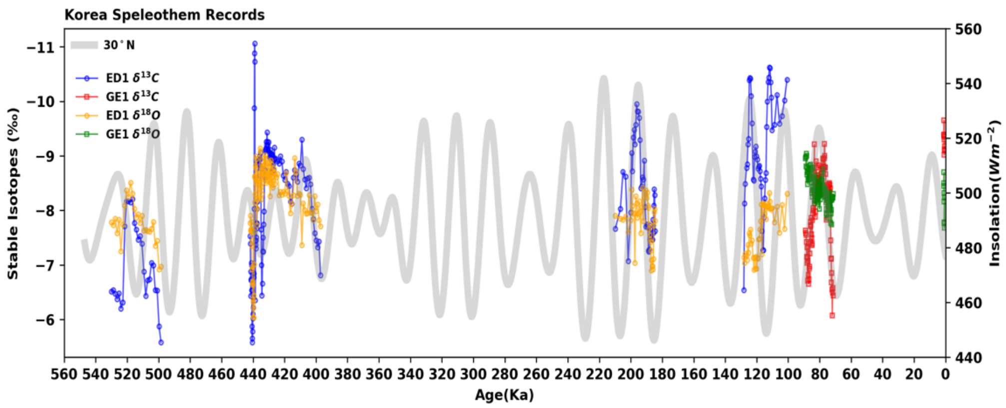

Fig. S1. *Speleothem ($\delta^{13}C$ and $\delta^{18}O$) records from Eden (ED) Cave and Gwaneum (GE) Cave stalagmites (ED1 and GE1, respectively) from South Korea. Refer to Jo et al* (2010, 2014) *for further details.*

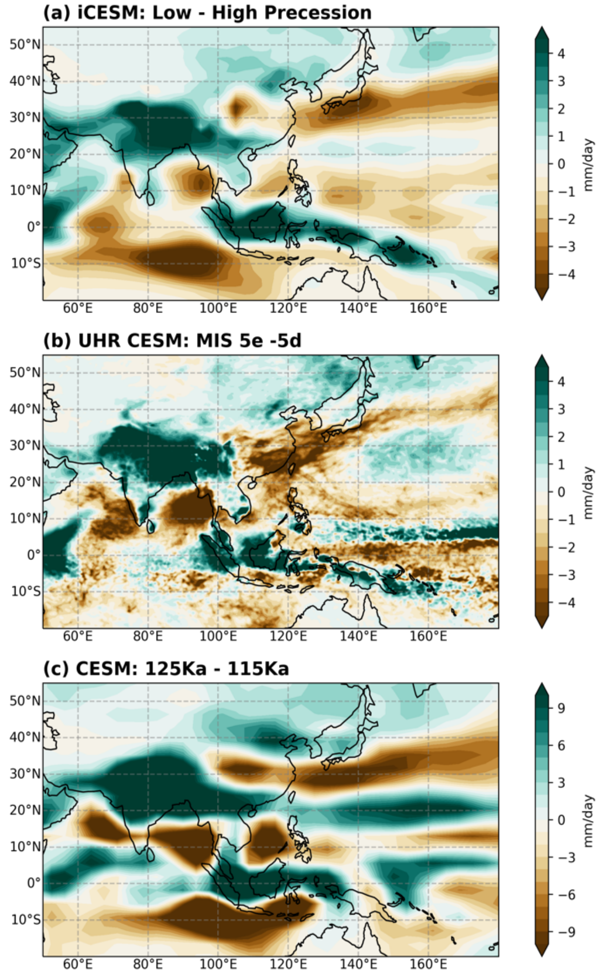

Fig. S2. *Summer mean precipitation differences for (a) Low – High precession from iCESM simulation (~2º horizontal resolution), (b) MIS5e – MIS5d from ultra-high-resolution (UHR) CESM simulations (~0.25º horizontal resolution), and (c) time slices for 125 ka – 115 ka from 3Ma transient simulation. (~3.75º horizontal resolution).*

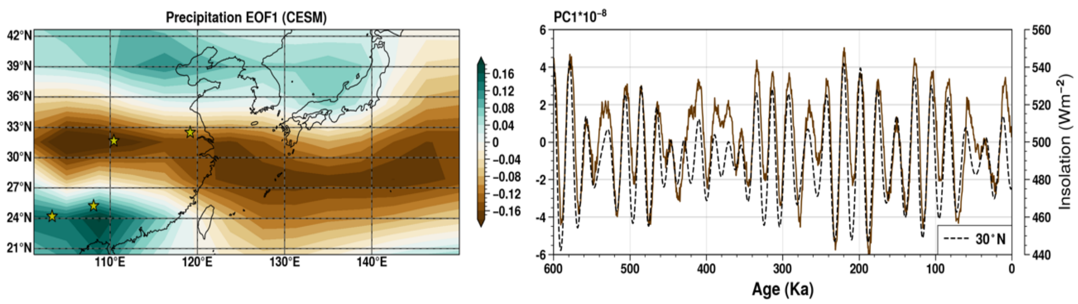

Fig. S3. *First empirical orthogonal function (EOF1) for annual mean precipitation (shaded, left panel) and corresponding principal component (PC1) (brown curve, right panel) for Eastern Asia using 3Ma transient simulation. The EOF analysis is based on the last 600 ka of the simulation. Major studied caves in China are marked by a yellow star symbol (left panel), refer to Figure 1. The black dashed curve represents summer insolation at 30°N (right panel).*

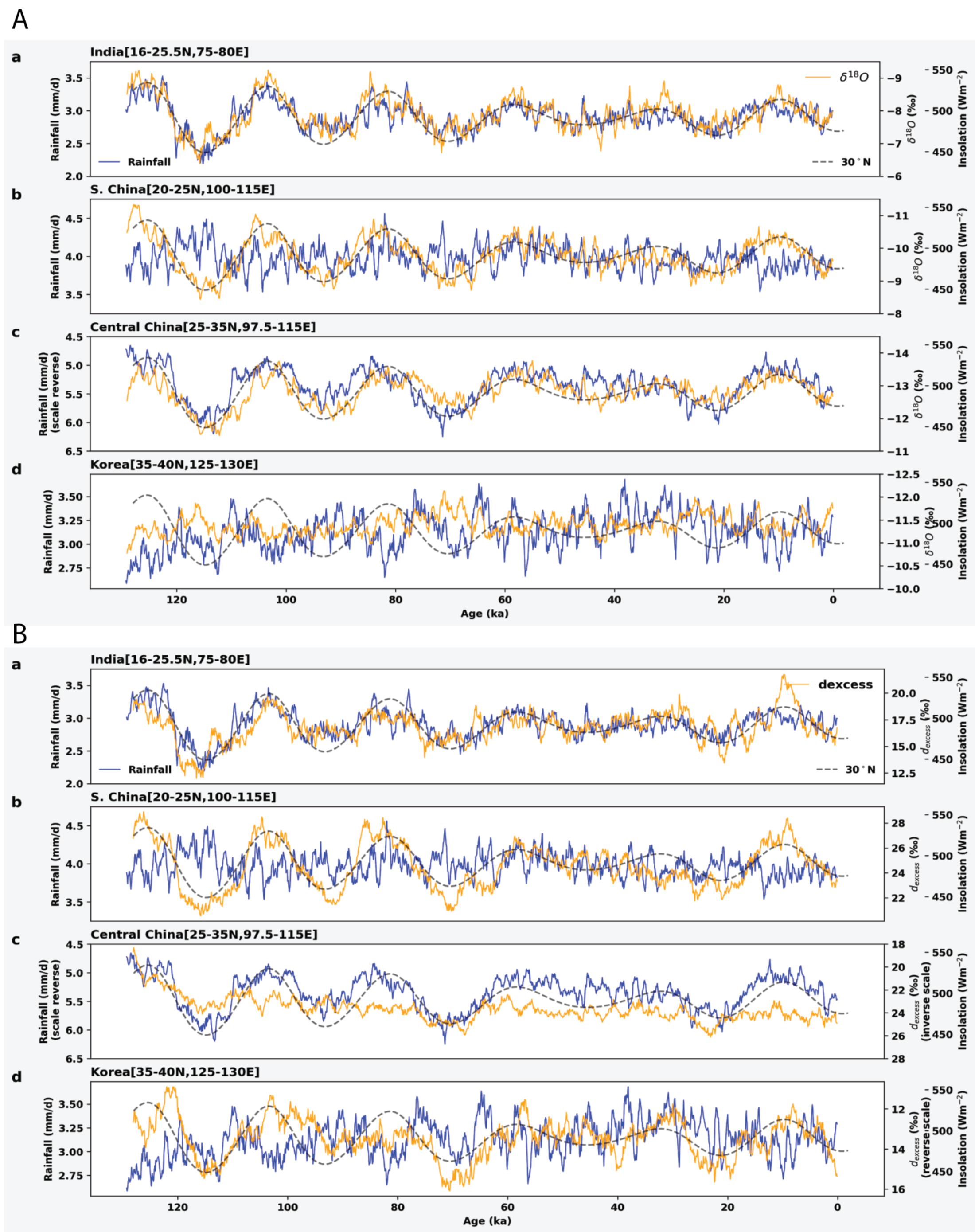

Fig. S4. *Simulated annual mean variations in precipitation (blue curves) for (a) India, (b) South (S.) China, (c) central China, and (d) Korea in the last 130ka from an orbitally forced transient simulation conducted with iCESM1.2. Orange curves in panel A (B) show precipitation-δ^{18}O (d-excess). Dashed black curves represent insolation (30 °N) insolation changes.*

Section S2

Beck's (Beck et al., 2018) ^{10}Be reconstruction corresponds well to simulated regional rainfall over the Loess area if we shift the ^{10}Be record by ~6 ka (Fig. S5c). The shifted ^{10}Be shows a higher correlation ($R^2 = 0.30$) with the simulated rainfall than the reported $R^2 = 0.16$ with the Sanbao $\delta^{18}O_c$ record. The ^{10}Be record (6 ka shifted) also matches well with Cryptomeria pollen records from Japan (Hayashi et al., 2021; Igarashi and Oba, 2006) (Figure 3c). Now, we understand that the precipitation and $\delta^{18}O_p$ spatial patterns as a grand dipole response to orbital forcing (Wen et al., 2024). The age shift may be justified as ^{10}Be age determination relies on the assumption that the Chinese speleothem-δ^{18}O record was controlled by regional EASM rainfall intensity. Moreover, our model simulations also do not support a temporally or spatially uniform relationship between EASM precipitation and $\delta^{18}O_p$ throughout the region on orbital timescales. For example, the Chinese speleothem-δ^{18}O does not align well with simulated rainfall over China but aligns better with rainfall over India (Fig. S5a and S5b).

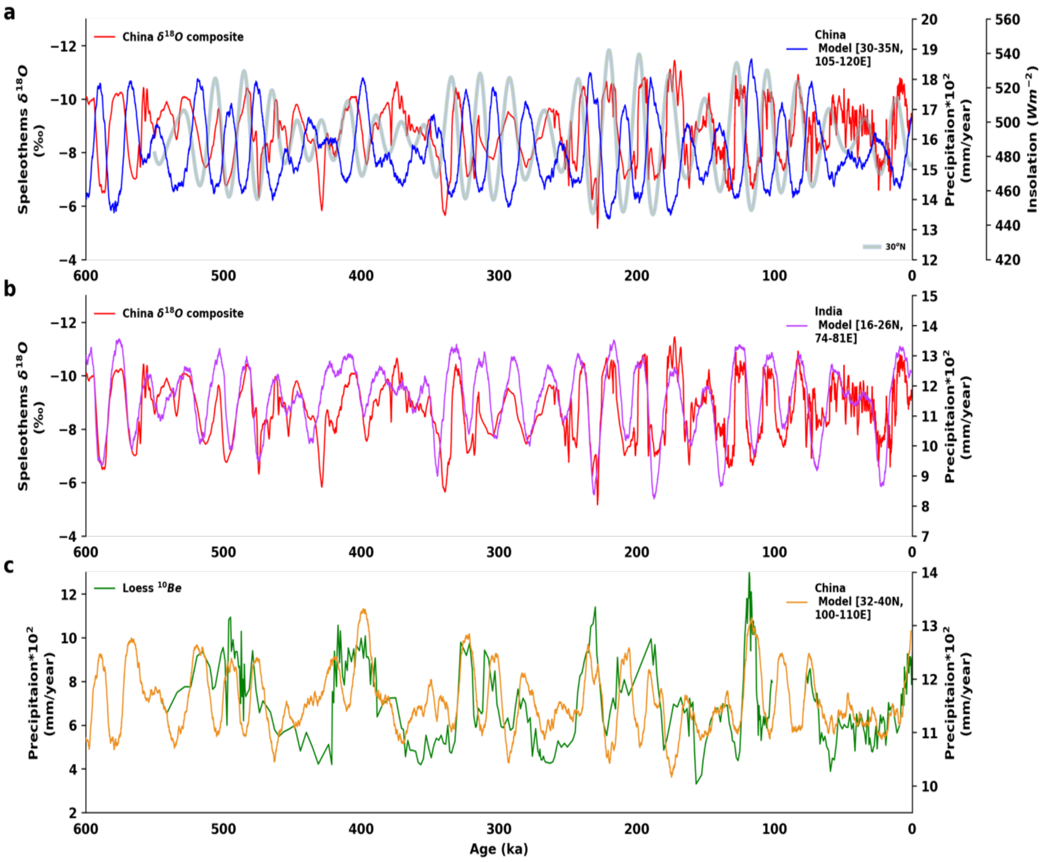

Fig. S5. *Comparison of simulated precipitation change by 3 Ma transient simulation (only the last 600 kyr are shown here) and proxies from (a) Eastern Asia and China speleothem-δ^{18}O composite record, (b) India and China speleothem-δ^{18}O composite record, and (c) China and Loess ^{10}Be record. Summer insolation at 30°N is shown in panel (a).*

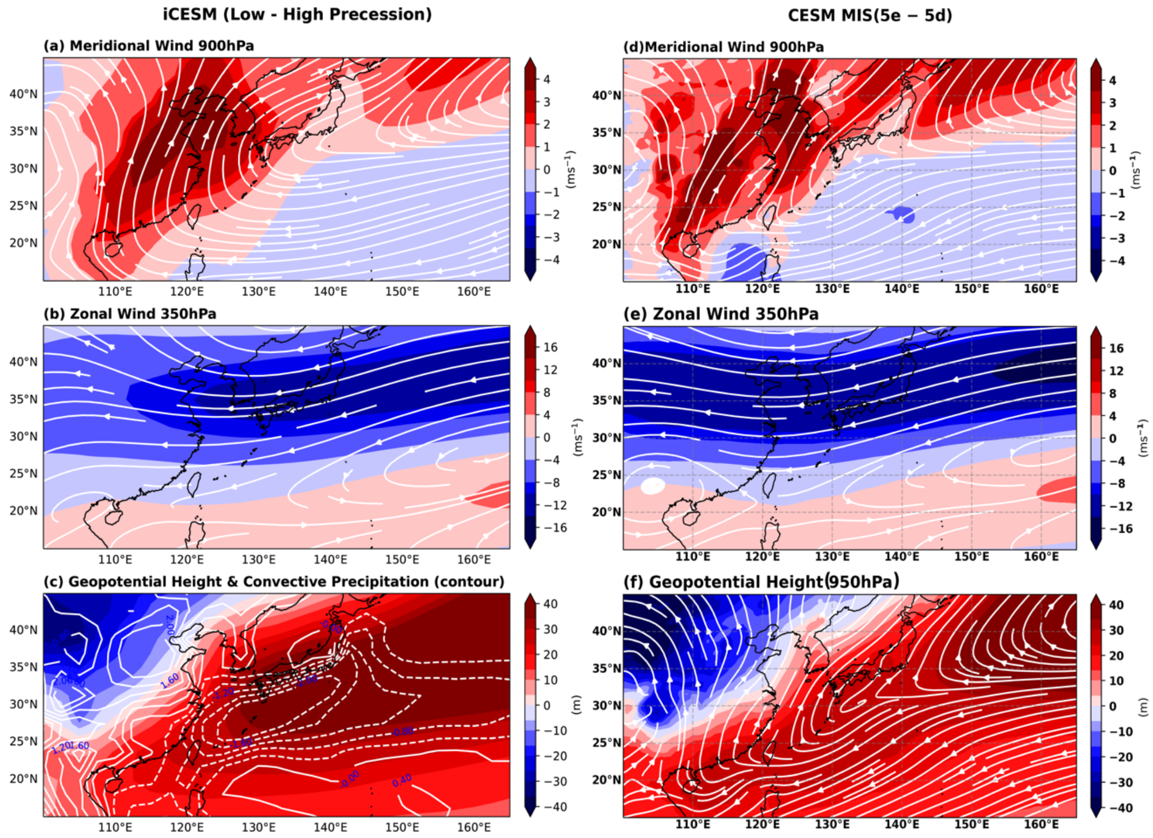

Fig. S6. *Differences between iCESM-130ka Pmin (Low) and Pmax (High) (left panels) and between hiresCESM MIS5e and MIS5d (right panels). (a)-(d) Meridional wind at 900 hPa (shading) and streamlines. (b)-(e) Zonal wind at 350 hPa (shading) and streamlines. (c) Geopotential height 950 hPa (shading) and convective precipitation (contour). (f) Geopotential height at 950 hPa (shading) and streamlines.*

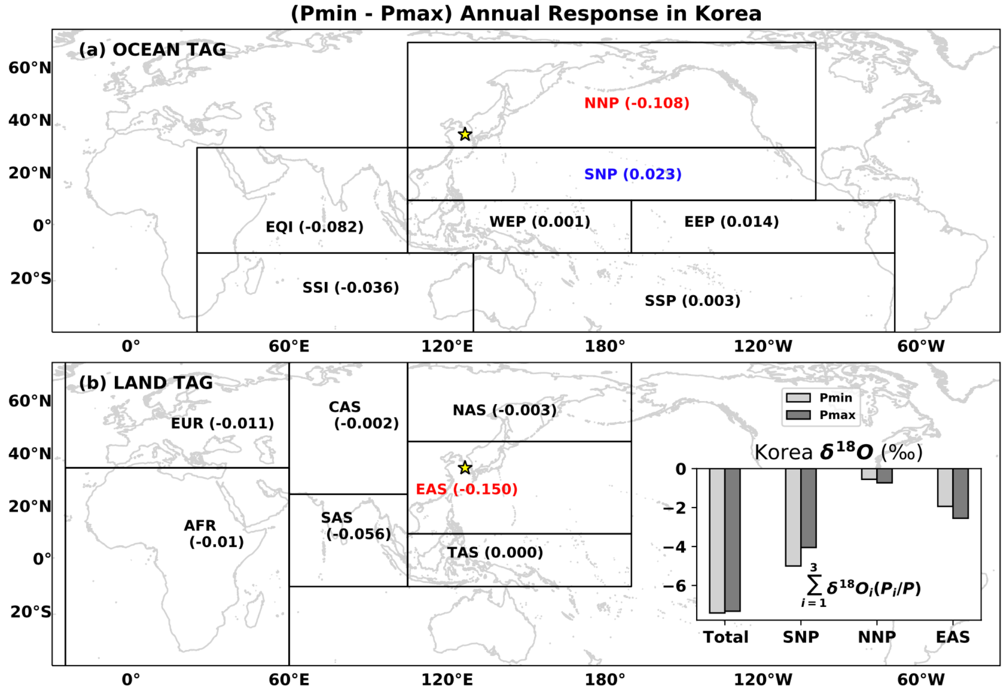

Fig. S7. *Differences in annual precipitation (mm/day) on the Korean Peninsula between Pmin and Pmax from various moisture sources over (a) ocean and (b) land. Color text is a major contributor to the Korean Peninsula (blue positive and red negative for P_{min} -P_{max}). Inset plot (lower right): the summer precipitation $\delta^{18}O$ in Korea from major and near-source contributors from Land (EAS) and the Ocean (SNP, NNP). "Total" represents the precipitation-$\delta^{18}O$ combination from all tag regions in Korea. Korea is marked by a yellow star.*

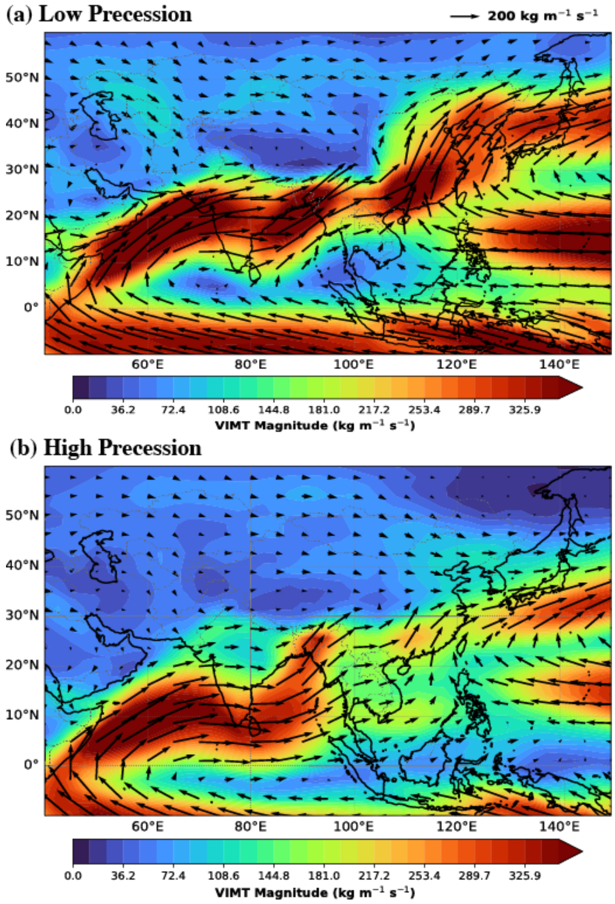

Fig. S8. *Vertically integrated moisture transport (VIMT) during boreal summer (JJA) under low precession (a) and high precession (b) conditions. VIMT magnitude (kg m^{-1} s^{-1}) showing the spatial distribution and intensity of moisture transport across Asia. Black arrows indicate VIMT vector direction and relative magnitude (reference vector: 200 kg m^{-1} s^{-1}).*

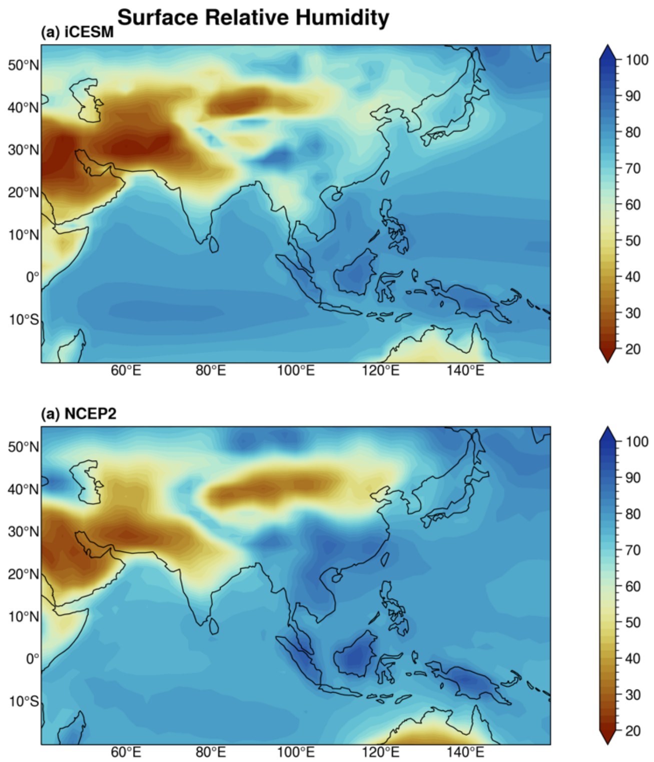

Fig. S9. *(a) Relative humidity simulated in iCESM for present day conditions in comparison to (b) NCEP2 reanalysis data for the last 40 years (accessed through APDRC OPeNDAP Server (http://apdrc.soest.hawaii.edu/index.php). Model captures the spatial pattern reasonably well, except lower humidity over the southeast Asian region.*

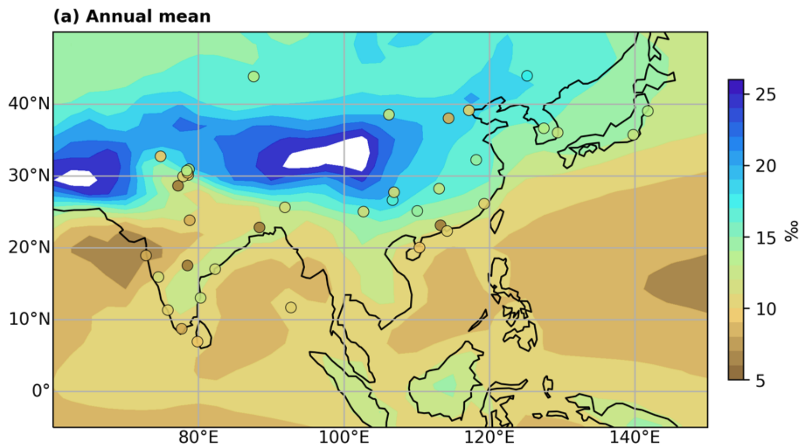

Fig. S10. *Present day iCESM simulated (shaded) d-excess and GNIP sites (circle) annual mean d-excess comparison.*

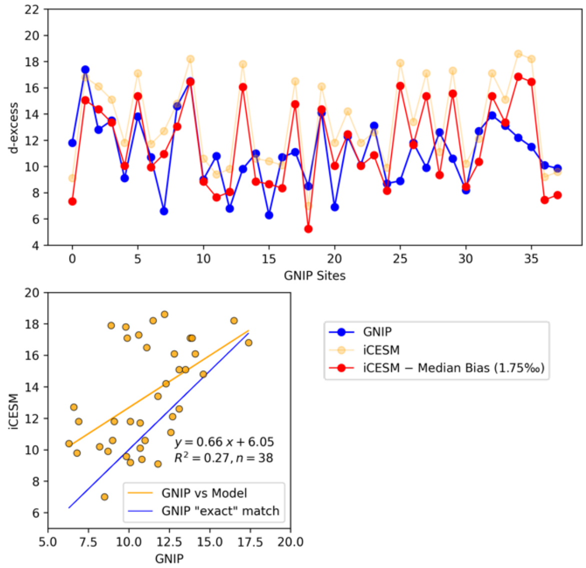

Fig. S11. *Upper panel shows the series of d-excess values for 38 Asian sites, GNIP (blue), iCESM (orange), and iCESM Median bias adjusted (red). Lower left panel shows the correlation between simulated and GNIP mean annual d-excess values for Asian sites. Note: All Asian GNIP sites are considered here, a screening has been applied, such as only the sites which have at least 2 years of data.*

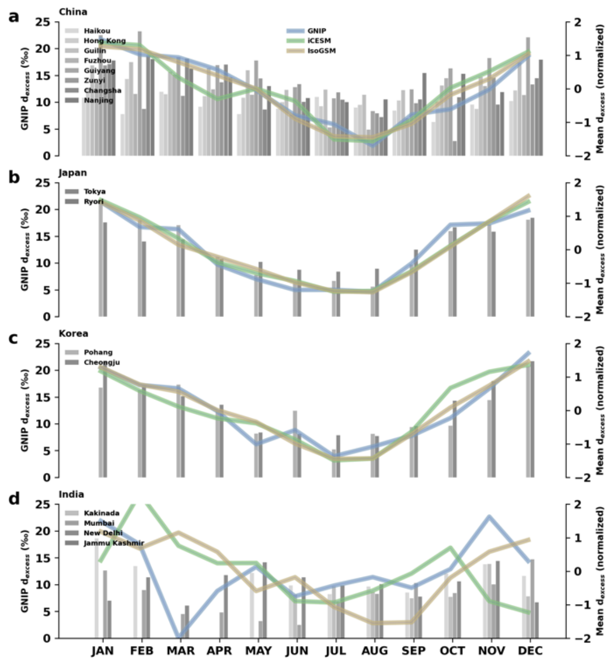

Fig. S12. *A comparison between the monthly climatology of d-excess from GNIP (light blue), iCESM simulation (light green), and IsoGSM2 (light brown) for some of the sites from China, Japan, Korea, and India. Gray bars show mean monthly d-excess for individual GNIP sites, gray shading represents site latitude from low to high (lighter to darker).*

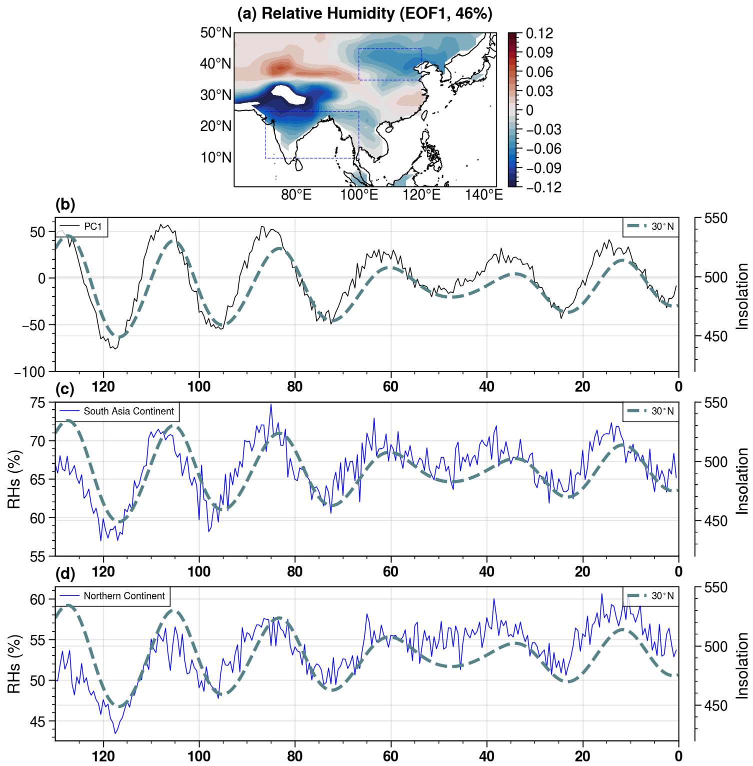

Fig. S13. *First empirical orthogonal function (EOF1(a)) and corresponding principal component (PC1, b) for the summer mean surface relative humidity for the 130 ka transient simulation on iCESM1.2. Temporal evolution of surface relative humidity over continental regions (c, d). The selected boxes are shown on the spatial map (a). The dashed curve represents summer insolation at 30°N. It is worth mentioning here that the EAS region in the tagging experiments covers the Chinese continent up to 45°N and 100°E.*

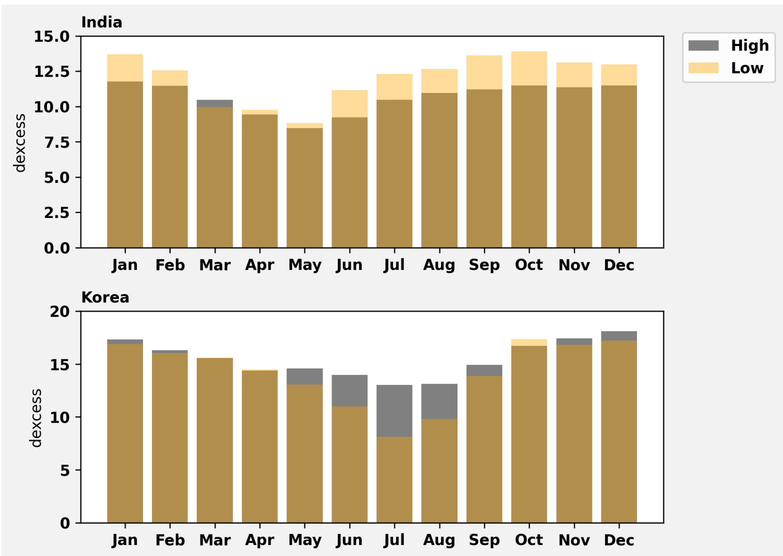

Fig. S14. *d-excess monthly climatology for low precession (Low) and high precession (High) over the Indian and the Korean regions.*

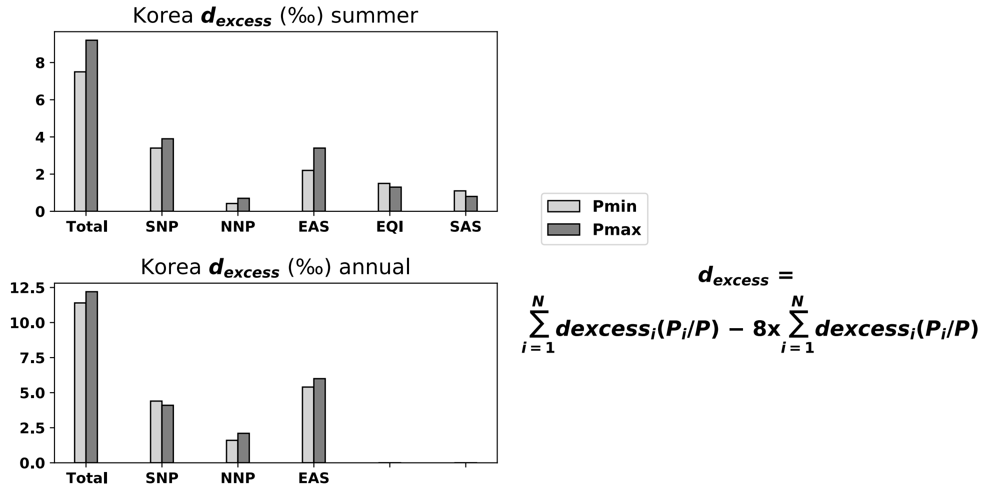

Fig. S15. *The summer and annual precipitation d-excess in Korea from major and near-source contributors from land and ocean. "Total" represents the d-excess from all tag regions to Korea.*

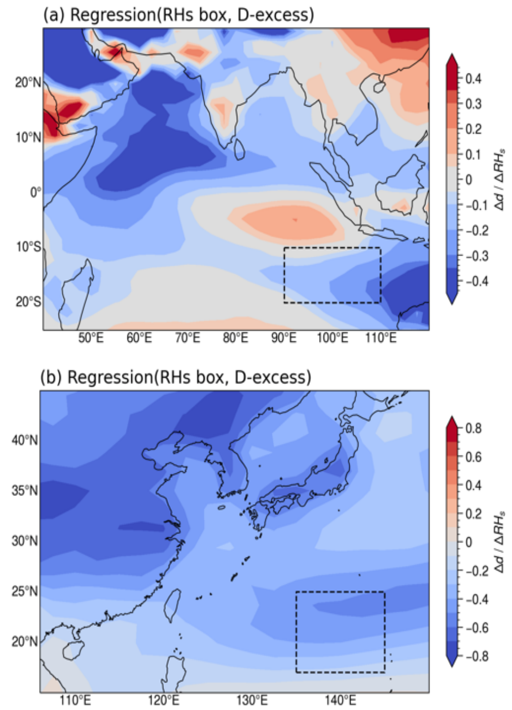

Fig. S16. *(a) Southern Indian Ocean (10-20°S; 90-110°E) and (b) Northwest Pacific Ocean (15-25°N; 135-145°E) surface relative (Rel.) humidity (RHs) regressed over the spatial d-excess(d) values for 130 ka transient simulation. The shading shows slope; Δd/ΔRHs.*

Table S1. *Details on the speleothem stable isotopes records and other proxies used in this study.*

Speleothem-$\delta^{18}O$ records			
	~ Ages (ka)	**Location (°N/°E)**	**Reference**
Korea			
1. Eden cave (ED1)	100 – 128, 184 – 209, 397 – 442, 498 – 530	37.10/128.50	(Jo et al., 2011, 2014)
2. Gwaneum cave (GE1)	0.70 – 1.18, 71 – 89	37.32/129.03	
China			
1. Composite	0 – 640	several	(Cheng et al., 2016)
Other proxy records	**~ Ages (ka)**	**Location (°N/°E)**	**Reference**
1. Loess ^{10}Be	0 – 84 and 107 – 550	34.43/107.12	(Beck et al., 2018)
2. U1427 pollen	0.65 – 551	35.96/134.43	(Hayashi et al., 2021)
3. Lake Biwa	1.8 – 134.3 and 0 - 430	~35/~136	(Hayashi et al., 2017; Tarasov et al., 2011)
Atmospheric CO_2			
1. EPICA Dome CO2	0-800	-75.1/158.72	(Lüthi et al., n.d.)

Table S2. *Tagging results. Blank spaces indicate tag regions not used in the total calculation (column "Total"), as they have no contribution to the anomalous $\delta^{18}O_p$ (Pmin- Pmax).*

(a) d18O

	SNP			NNP			EAS			EQI			SAS			Total	
Annual	Pi	d18Oi	d18Oi*(Pi/P)	Pi	d18Oi	d18Oi*(Pi/P)	Pi	d18Oi	d18Oi*(Pi/P)	Pi	d18Oi	d18Oi*(Pi/P)	Pi	d18Oi	d18Oi*(Pi/P)	P	d18O
Pmax	0.99	-11.26	-3.43	0.44	-4.49	-0.62	1.31	-5.32	-2.16	0.2773	-16.81	-1.44	0.215	-16.67	-1.11	3.24	-8.76
Pmin	1.01	-12.31	-4.34	0.34	-4.07	-0.48	1.16	-4.13	-1.68	0.1955	-19.36	-1.32	0.159	-19.09	-1.06	2.86	-8.88
Pmin - Pmax	0.023		-0.91			0.14			0.48			0.12			0.05	-0.37	-0.12
Pmax	0.99	-11.26	-4.05	0.44	-4.49	-0.73	1.31	-5.32	-2.55							2.74	-7.32
Pmin	1.01	-12.31	-4.96	0.34	-4.07	-0.55	1.16	-4.13	-1.91							2.51	-7.42
Pmin - Pmax	0.023		-0.91			0.18			0.63							-0.23	-0.09
Summer	Pi	d18Oi	d18Oi*(Pi/P)	Pi	d18Oi	d18Oi*(Pi/P)	Pi	d18Oi	d18Oi*(Pi/P)	Pi	d18Oi	d18Oi*(Pi/P)	Pi	d18Oi	d18Oi*(Pi/P)	P	d18O
Pmax	1.60	-7.48	-2.41	0.37	-4.18	-0.31	1.76	-4.67	-1.66	0.73	-10.26	-1.50	0.502	-9.54	-0.97	4.96	-6.85
Pmin	2.00	-5.76	-2.20	0.23	-5.53	-0.24	1.87	-3.78	-1.35	0.63	-13.35	-1.61	0.518	-12.56	-1.24	5.24	-6.63
Pmin - Pmax	0.400		0.22			0.07			0.31			-0.11			-0.28	0.28	0.22

(b) dD

	SNP			NNP			EAS			EQI			SAS			Total	
Annual	Pi	dDi	dDi*(Pi/P)	Pi	dDi	dDi*(Pi/P)	Pi	dDi	dDi*(Pi/P)	Pi	dDi	dDi*(Pi/P)	Pi	dDi	dDi*(Pi/P)	P	d18O
Pmax	0.99	-78.75	-28.33	0.44	-22.89	-3.71	1.31	-30.03	-14.36							2.74	-46.40
Pmin	1.01	-87.61	-35.27	0.34	-20.25	-2.72	1.16	-21.30	-9.86							2.51	-47.85
Pmin - Pmax	0.023		-6.94			0.99			4.49							-0.23	-1.45
	SNP			NNP			EAS			EQI			SAS			Total	
Summer	Pi	dDi	dDi*(Pi/P)	Pi	dDi	dDi*(Pi/P)	Pi	dDi	dDi*(Pi/P)	Pi	dDi	dDi*(Pi/P)	Pi	dDi	dDi*(Pi/P)	P	d18O
Pmax	1.60	-49.11	-15.85	0.37	-25.20	-1.88	1.76	-28.64	-10.17	0.73	-74.25	-10.86	0.502	-68.43	-6.93	4.96	-45.69
Pmin	2.00	-38.14	-14.56	0.23	-35.55	-1.53	1.87	-24.57	-8.74	0.63	-95.66	-11.54	0.518	-89.5	-8.85	5.24	-45.21
Pmin - Pmax	0.400		1.29			0.35			1.42			-0.67			-1.92	0.28	0.48

(c) d-excess

	SNP			NNP			EAS			EQI			SAS			Total	
Annual	Pi	dex_i	dex_i*(Pi/P)	Pi	dex_i	dex_i*(Pi/P)	Pi	dex_i	dex_i*(Pi/P)	Pi	dex_i	dex_i*(Pi/P)	Pi	dex_i	dex_i*(Pi/P)	P	dexc
Pmax	0.99	11.33	4.08	0.44	13.00	2.11	1.31	12.55	6.00							2.74	12.19
Pmin	1.01	10.87	4.38	0.34	12.29	1.65	1.16	11.76	5.45							2.51	11.47
Pmin - Pmax	0.023		0.30			-0.46			-0.55							-0.23	-0.71
	SNP			NNP			EAS			EQI			SAS			Total	
Summer	Pi	dex_i	dex_i*(Pi/P)	Pi	dex_i	dex_i*(Pi/P)	Pi	dex_i	dex_i*(Pi/P)	Pi	dex_i	dex_i*(Pi/P)	Pi	dex_i	dex_i*(Pi/P)	P	dexc
Pmax	1.60	10.73	3.46	0.37	8.20	0.61	1.76	8.70	3.09	0.73	7.83	1.15	0.502	7.89	0.80	4.96	9.11
Pmin	2.00	7.94	3.03	0.23	8.71	0.37	1.87	5.67	2.02	0.63	11.14	1.34	0.518	10.98	1.09	5.24	7.85
Pmin - Pmax	0.400		-0.43			-0.24			-1.07		3.31				0.29	0.28	-1.26

Table S3.: *Korean Speleothem-$\delta^{18}O$ records.*

(a) Eden Cave		(b) Gwaneum Cave	
Age (ka BP)	**$\delta^{18}O$ (‰, VPDB)**	**Age (ka BP)**	**δ18O (‰, VPDB)**
128.19	-7.14	89.00	-8.95
127.77	-7.04	88.83	-8.98
127.34	-7.21	88.66	-8.81
126.49	-7.18	88.49	-9.04
126.06	-7.09	88.32	-9.00
125.63	-7.37	88.15	-8.78
125.21	-7.22	87.98	-8.66
124.78	-7.58	87.81	-8.70
124.36	-7.54	87.64	-8.48
123.93	-7.65	87.47	-8.57
123.50	-7.39	87.30	-8.70
123.08	-7.45	87.13	-8.56
122.22	-7.13	86.96	-8.76
121.80	-6.91	86.79	-8.67
121.37	-7.13	86.62	-8.63
120.94	-6.93	86.45	-8.60
120.52	-7.15	86.28	-8.58
120.09	-6.93	86.11	-8.82
119.66	-7.13	85.94	-8.84
119.24	-7.12	85.77	-8.77
118.81	-7.47	85.60	-8.74
118.39	-7.48	85.43	-8.52
117.96	-7.65	85.26	-8.78
117.53	-7.80	85.09	-8.61
117.11	-8.11	84.92	-8.37
116.68	-7.20	84.75	-8.32
116.25	-8.13	84.58	-8.25
115.83	-8.12	84.41	-8.43
115.40	-8.10	84.24	-8.79
114.97	-7.94	84.07	-8.58
114.55	-8.08	83.90	-8.59
114.12	-7.84	83.73	-8.60
113.70	-8.12	83.56	-8.34
113.27	-8.07	83.39	-8.13
112.84	-8.08	83.22	-8.27
112.42	-8.04	83.05	-8.39
111.99	-8.32	82.88	-8.18
111.56	-8.16	82.71	-8.40
111.14	-8.02	82.54	-8.64

110.71	-8.04	82.37	-8.52
110.28	-8.04	82.20	-8.49
108.70	-7.78	82.03	-8.37
107.12	-8.07	81.86	-8.32
105.54	-7.59	81.69	-8.38
103.96	-8.10	81.52	-8.17
102.38	-7.66	81.35	-8.21
100.80	-8.31	81.18	-8.24
		81.01	-8.25
209.89	-7.90	80.84	-8.14
206.62	-7.85	80.67	-8.27
204.98	-7.83	80.50	-8.27
203.35	-7.89	80.33	-8.53
201.71	-7.60	80.16	-8.03
200.08	-7.82	79.99	-8.36
199.54	-8.38	79.82	-8.47
199.01	-8.08	79.65	-8.20
198.47	-7.94	79.48	-8.29
197.93	-7.95	79.31	-8.40
197.40	-7.04	79.14	-8.30
196.86	-8.26	78.97	-8.57
196.33	-8.13	78.80	-8.56
195.79	-7.87	78.63	-8.63
195.26	-7.94	78.46	-8.54
194.72	-8.17	78.29	-8.46
194.18	-7.97	78.12	-8.35
193.65	-7.58	77.95	-8.75
193.11	-8.06	77.78	-8.41
192.58	-8.42	77.61	-8.43
192.04	-7.80	77.44	-8.34
191.51	-8.23	77.27	-8.36
190.97	-8.32	77.10	-8.37
190.43	-8.37	76.93	-8.30
189.90	-8.23	76.76	-8.39
189.36	-8.33	76.59	-8.25
189.10	-8.09	76.42	-8.38
188.83	-8.05	76.25	-8.25
188.57	-7.66	76.08	-8.15
188.31	-7.75	75.91	-8.03
188.04	-7.55	75.74	-7.94
187.78	-7.47	75.57	-7.92
187.51	-7.42	75.40	-8.19
187.25	-7.26	75.23	-7.86

186.98	-6.90	75.06	-8.29
186.72	-7.09	74.89	-8.22
186.45	-6.98	74.72	-8.18
186.19	-6.98	74.55	-8.21
185.93	-6.92	74.38	-8.31
185.66	-7.11	74.21	-8.23
185.40	-7.72	74.04	-8.15
185.13	-7.97	73.87	-8.33
184.87	-8.03	73.70	-8.10
184.60	-7.81	73.53	-8.02
		73.36	-8.11
441.84	-7.77	73.19	-8.05
441.72	-7.90	73.02	-7.77
441.60	-7.63	72.85	-7.94
441.48	-7.64	72.68	-8.19
441.36	-7.62	72.51	-8.01
441.24	-7.61	72.34	-7.74
441.13	-7.66	72.17	-8.20
441.01	-7.79	72.00	-8.25
440.89	-7.35	71.83	-8.23
440.77	-7.44	71.66	-8.24
440.65	-6.92	71.49	-8.30
440.53	-6.97		
440.42	-6.67	1.18	-8.45
440.30	-6.70	1.12	-8.50
440.18	-6.63	1.06	-8.70
440.06	-6.37	1.00	-8.16
439.94	-6.04	0.94	-8.32
439.82	-6.32	0.88	-7.77
439.71	-6.21	0.82	-8.24
439.59	-6.44	0.76	-7.68
439.47	-6.03	0.70	-7.78
439.35	-7.01		
439.23	-7.61		
439.11	-8.63		
439.00	-8.60		
438.88	-8.15		
438.64	-8.30		
438.52	-8.83		
438.40	-8.78		
438.17	-8.99		
438.05	-8.50		
437.93	-8.94		

437.81	-8.56
437.69	-8.67
437.58	-7.73
437.46	-8.21
437.22	-8.03
436.99	-8.58
436.76	-8.51
436.52	-8.54
436.29	-8.22
436.06	-8.40
435.82	-8.69
435.59	-9.14
435.36	-9.08
435.12	-8.66
434.89	-8.20
434.66	-8.43
434.42	-8.30
434.19	-8.79
433.96	-8.72
433.72	-8.83
433.49	-8.52
433.26	-8.96
433.02	-8.63
432.79	-8.85
432.56	-8.69
432.32	-9.01
432.09	-8.68
431.86	-8.95
431.62	-8.51
431.39	-8.62
431.16	-8.55
430.92	-8.61
430.69	-8.69
430.46	-8.87
430.22	-8.65
429.99	-8.81
429.76	-8.89
429.52	-8.55
429.29	-8.26
429.06	-8.67
428.82	-8.50
428.59	-8.92
428.36	-8.74

428.12	-8.84
427.89	-8.60
427.66	-8.47
427.42	-8.42
427.19	-8.63
426.96	-8.71
426.72	-8.77
426.49	-8.68
426.26	-8.49
425.35	-8.61
424.44	-8.67
423.53	-8.28
422.63	-8.34
421.72	-8.29
420.81	-8.34
419.90	-8.31
418.99	-8.69
418.09	-8.36
417.18	-8.27
416.27	-7.95
415.36	-8.12
414.45	-8.28
413.55	-8.96
412.64	-8.70
411.73	-8.27
410.82	-8.31
409.91	-8.29
409.00	-7.36
408.10	-8.13
407.19	-8.01
406.28	-7.94
405.37	-7.95
404.46	-8.28
403.56	-7.96
402.65	-7.96
401.74	-7.82
400.83	-8.26
399.92	-7.99
399.02	-8.11
398.11	-7.82
397.20	-7.71
529.99	-7.78

528.78	-7.73
527.57	-7.85
526.36	-7.58
525.15	-7.83
523.94	-7.25
522.73	-7.74
521.52	-8.09
520.31	-8.37
519.10	-8.24
517.89	-8.51
516.68	-8.31
515.47	-8.03
514.26	-7.87
513.04	-7.93
511.83	-7.77
510.62	-7.90
509.41	-7.63
508.20	-7.64
506.99	-7.62
505.78	-7.61
504.57	-7.66
503.36	-7.79
502.15	-7.35
500.94	-7.44
499.73	-6.92
498.52	-6.97

SI References

Beck, J. W., Zhou, W., Li, C., Wu, Z., White, L., Xian, F., Kong, X., and An, Z.: A 550,000-year record of East Asian monsoon rainfall from ^{10}Be in loess, Science, 360, 877–881, https://doi.org/10.1126/science.aam5825, 2018.

Cheng, H., Edwards, R. L., Sinha, A., Spötl, C., Yi, L., Chen, S., Kelly, M., Kathayat, G., Wang, X., Li, X., Kong, X., Wang, Y., Ning, Y., and Zhang, H.: The Asian monsoon over the past 640,000 years and ice age terminations, Nature, 534, 640–646, https://doi.org/10.1038/nature18591, 2016.

Hayashi, R., Takahara, H., Inouchi, Y., Takemura, K., and Igarashi, Y.: Vegetation and endemic tree response to orbital-scale climate changes in the Japanese archipelago during the last glacial–interglacial cycle based on pollen records from Lake Biwa, western Japan, Review of Palaeobotany and Palynology, 241, 85–97, https://doi.org/10.1016/j.revpalbo.2017.02.008, 2017.

Hayashi, R., Sagawa, T., Irino, T., and Tada, R.: Orbital-scale vegetation-ocean-atmosphere linkages in western Japan during the last 550 ka based on a pollen record from the IODP site U1427 in the Japan Sea, Quaternary Science Reviews, 267, 107103, https://doi.org/10.1016/j.quascirev.2021.107103, 2021.

Igarashi, Y. and Oba, T.: Fluctuations in the East Asian monsoon over the last 144ka in the northwest Pacific based on a high-resolution pollen analysis of IMAGES core MD01-2421, Quaternary Science Reviews, 25, 1447–1459, https://doi.org/10.1016/j.quascirev.2005.11.011, 2006.

Jo, K., Woo, K. S., Cheng, H., Edwards, L. R., Wang, Y., Kim, R., and Jiang, X.: Textural and carbon isotopic evidence of monsoonal changes recorded in a composite-type speleothem from Korea since MIS 5a, Quat. res., 74, 100–112, https://doi.org/10.1016/j.yqres.2010.04.005, 2010.

Jo, K., Woo, K. S., Lim, H. S., Cheng, H., Edwards, R. L., Wang, Y., Jiang, X., Kim, R., Lee, J. I., Yoon, H. I., and Yoo, K.-C.: Holocene and Eemian climatic optima in the Korean Peninsula based on textural and carbon isotopic records from the stalagmite of the Daeya Cave, South Korea, Quaternary Science Reviews, 30, 1218–1231, https://doi.org/10.1016/j.quascirev.2011.02.012, 2011.

Jo, K., Woo, K. S., Yi, S., Yang, D. Y., Lim, H. S., Wang, Y., Cheng, H., and Edwards, R. L.: Mid-latitude interhemispheric hydrologic seesaw over the past 550,000 years, Nature, 508, 378–382, https://doi.org/10.1038/nature13076, 2014.

Lüthi, D., Le Floch, M., Bereiter, B., Blunier, T., Barnola, J. M., Siegenthaler, U., Raynaud, D., Jouzel, J., Fischer, H., Kawamura, K., and Stocker, T. F.: NOAA/WDS Paleoclimatology - EPICA Dome C - 800KYr CO2 Data, https://doi.org/10.25921/XGZS-GD10, n.d.

Tarasov, P. E., Nakagawa, T., Demske, D., Österle, H., Igarashi, Y., Kitagawa, J., Mokhova, L., Bazarova, V., Okuda, M., Gotanda, K., Miyoshi, N., Fujiki, T., Takemura, K., Yonenobu, H., and Fleck, A.: Progress in the reconstruction of Quaternary climate dynamics in the Northwest Pacific: A new modern analogue reference dataset and its application to the 430-kyr pollen record from Lake Biwa, Earth-Science Reviews, 108, 64–79, https://doi.org/10.1016/j.earscirev.2011.06.002, 2011.

Wen, Q., Liu, Z., Jing, Z., Clemens, S. C., Wang, Y., Yan, M., Ning, L., and Liu, J.: Grand dipole response of Asian summer monsoon to orbital forcing, npj Clim Atmos Sci, 7, 202, https://doi.org/10.1038/s41612-024-00749-4, 2024.